PERGAMON

International Journal of Heat and Mass Transfer 45 (2002) 2221–2228

International Journal of HEAT and MASS TRANSFER

www.elsevier.com/locate/ijhmt

Onset of Darcy–Bénard convection using a thermal non-equilibrium model

Nurzahan Banu, D.A.S. Rees *

Department of Mechanical Engineering, University of Bath, Claverton Down, Bath, BA2 7AY, UK

Received 7 March 2000; received in revised form 29 October 2001

Abstract

In this paper we use a two-field model for the separate modelling of the solid and fluid phase temperature fields in a fluid-saturated porous medium, and, in particular, we consider how the onset criterion for convection in a horizontal layer is affected by the adoption of such a model. In general we find that both the critical Rayleigh number and wavenumber are modified by the presence of thermal non-equilibrium effects. It is shown that the well-known result of Lapwood [Proc. Cambridge Philos. Soc. 44 (1948) 508] which corresponds to local thermal equilibrium (LTE), is recovered when taking the thermal equilibrium limit of the non-equilibrium analysis.

We also present asymptotic solutions for both small and large values of H the inter-phase heat transfer coefficient, H, and compare this with the numerical solutions. For intermediate values of H we find that the critical wavenumber is always larger than π, the critical value for the LTE case. In some cases this critical wavenumber may be very large compared with π. © 2002 Published by Elsevier Science Ltd.

1. Introduction

In this paper we consider the onset of convection in a porous layer heated from below, with emphasis on how the criterion for the onset of convection is modified when the solid and fluid phases are not in local thermal equilibrium (LTE). This study forms part of a series of articles investigating non-equilibrium effects in free convective flows in porous media by Rees and Pop [2,3] and Rees [4].

Nield and Bejan [5] state the equations which are generally regarded as modelling unsteady heat transfer in a saturated porous medium where LTE does not apply. Instead of having a single energy equation which describes the common temperature of the saturated medium (the one-field model), two equations are used to model the fluid and solid phases separately (the two-field model). In the two-field model the energy equations are coupled by means of terms which account for the heat lost to or gained from the other phase. Quintard et al. [6] describe this as the simplest form that reflects the concept of two macroscopic media. Thus the inter-phase heat transfer is modelled by a heat transfer coefficient, h, whose value depends on the nature of the porous matrix and the saturating fluid. In a recent review Vafai and Amiri [7] discuss possible values of this coefficient which has been the subject of intense experimental interest. Large values of h correspond to a rapid transfer of heat between the phases, and therefore such values are taken to correspond to LTE. Conversely, small values of h give rise to relatively strong non-equilibrium effects.

The two-field model is now being used extensively, especially in the realm of forced convective transport. Typical situations which require the use of the two-field model include hyper-porous materials (see [8] and references cited therein), and media in which there is a significant difference in conductivities between the phases (see [9], for example). Carbonell and Whitaker [10] give conditions in terms of length and time scales which ensure that local thermal non-equilibrium effects remain significant.

First examined by Lapwood [1] and Horton and Rogers [11], the Darcy model with LTE forms what is

* Corresponding author. Tel.: +44-1225-826-775; fax: +44-1225-826-928.

E-mail address: d.a.s.rees@bath.ac.uk (D.A.S. Rees).

0017-9310/02/$ - see front matter © 2002 Published by Elsevier Science Ltd.
PII: S0017-9310(01)00331-3

Nomenclature

c	specific heat
d	depth of the convection layer
g	gravity
h	inter-phase heat transfer coefficient
H	scaled inter-phase heat transfer coefficient
k	wavenumber
K	permeability
LTE	local thermal equilibrium
p	pressure
R	Darcy–Rayleigh number
t	time
x, y	Cartesian coordinates

Greek symbols

α	diffusivity ratio
β	coefficient of cubical expansion
ρ	density
μ	coefficient of viscosity
κ	diffusivity
γ	porosity-modified conductivity ratio
ϵ	porosity
ψ	streamfunction
θ	scaled temperature of the fluid phase
ϕ	scaled temperature of the solid phase

Superscripts and subscripts

$\bar{}$	dimensional
f	fluid
l	lower
s	solid
u	upper

perhaps the simplest linearised stability analysis based on a partial differential system of equations. When non-equilibrium effects are included, the linearised analysis is modified, although it is still possible to proceed entirely analytically with the exception of being able to write down a simple closed-form expression for the minimising wavenumber. We show that the LTE limit of the non-LTE analysis does indeed recover the classical LTE results of Lapwood [1]. In both the LTE ($h \to \infty$) and non-LTE ($h \to 0$) limits the critical wavenumber tends towards π, but it is above this at intermediate values of h. Although some finite difference computations of strongly nonlinear convection have been undertaken by Combarnous [12], this very early work corresponds to a fixed Rayleigh number of 200 and a unit aspect ratio cavity. Here we concentrate on the onset problem in order to determine the detailed context into which may be set the computations of [8].

2. Governing equations and analysis

The equations governing Darcy–Boussinesq convection in a saturated porous medium are usually studied by first invoking the assumption that the solid and fluid phases of the medium are local thermal equilibrium. In this paper we study one particular case where a two-temperature model of microscopic heat transfer applies. The governing equations are

$$\frac{\partial \bar{u}}{\partial \bar{x}} + \frac{\partial \bar{v}}{\partial \bar{y}} = 0, \tag{1a}$$

$$\bar{u} = -\frac{K}{\mu}\frac{\partial \bar{p}}{\partial \bar{x}}, \tag{1b}$$

$$\bar{v} = -\frac{K}{\mu}\frac{\partial \bar{p}}{\partial \bar{y}} + \frac{\rho_f g \beta K}{\mu}(T_f - T_u), \tag{1c}$$

$$\epsilon(\rho c)_f \frac{\partial T_f}{\partial t} + (\rho c)_f \underline{\bar{u}}.\nabla T_f = \epsilon k_f \nabla^2 T_f + h(T_s - T_f), \tag{1d}$$

$$(1-\epsilon)(\rho c)_s \frac{\partial T_s}{\partial t} = (1-\epsilon)k_s \nabla^2 T_s - h(T_s - T_f), \tag{1e}$$

see Nield and Bejan [5]; more complicated scenarios have been reviewed by Quintard [13]. Here, $\bar{u}$ and $\bar{v}$ are the fluid flux velocities in the horizontal and vertical spanwise directions, respectively, and $\bar{x}$ and $\bar{y}$ are the corresponding Cartesian coordinates. Further $\bar{t}$ is time, the pressure is $\bar{p}$ and the temperature is T, where the f and s subscripts denote the fluid and solid phases, respectively. The following are the other fluid and medium properties: K is the permeability, μ the fluid viscosity, ρ density, c the specific heat, β the coefficient of cubical expansion, ϵ the porosity and k the thermal conductivity. We consider Darcy–Bénard convection in a layer of depth, d, where the lower surface is held at a temperature, T_l, while the upper surface is at T_u. We note that, in the absence of LTE, the question of appropriate boundary conditions for the temperature fields may become more difficult to answer (see [14], for example), but, for now, we assume that the phases have identical temperatures at the bounding surfaces.

Eqs. (1a)–(1e) may be non-dimensionalised using the transformations

$$(\bar{x}, \bar{y}) = d(x, y), \tag{2a}$$

$$(\bar{u}, \bar{v}) = \frac{\epsilon k_f}{(\rho c)_f d}(u, v), \tag{2b}$$

$$\bar{p} = \frac{k_f \mu}{(\rho c)_f K} p, \tag{2c}$$

$$T_f = (T_l - T_u)\theta + T_u, \tag{2d}$$

$$T_s = (T_l - T_u)\phi + T_u, \tag{2e}$$

$$\bar{t} = \frac{(\rho c)_f}{k_f} d^2 t. \tag{2f}$$

A further simplification is afforded by introducing the streamfunction, ψ, according to $u = -\psi_y$ and $v = \psi_x$; Eqs. (1a)–(1e) become

$$\psi_{xx} + \psi_{yy} = R\theta_x, \tag{3a}$$

$$\theta_t - \psi_y\theta_x + \psi_x\theta_y = \theta_{xx} + \theta_{yy} + H(\phi - \theta), \tag{3b}$$

$$\alpha\phi_t = \phi_{xx} + \phi_{yy} + \gamma H(\theta - \phi), \tag{3c}$$

where

$$R = \frac{\rho_f g\beta(T_l - T_u)Kd}{\epsilon\mu\kappa_f}, \quad \gamma = \frac{\epsilon k_f}{(1-\epsilon)k_s},$$
$$H = \frac{hd^2}{\epsilon k_f}, \quad \alpha = \frac{(\rho c)_s}{(\rho c)_f}\frac{k_f}{k_s} = \frac{\kappa_f}{\kappa_s} \tag{4}$$

are the Darcy–Rayleigh number based on the fluid properties, a porosity-modified conductivity ratio, a scaled inter-phase heat transfer coefficient, and a diffusivity ratio.

Given the form of (2a)–(2f), the boundary conditions for (3a)–(3c) are that $\psi = 0$ and $\theta = \phi = 1$ on $y = 0$, the lower surface, and that $\psi = \theta = \phi = 0$ on $y = 1$, the upper surface. The conduction profile, whose stability forms the subject of this paper, is given by

$$\psi = 0, \quad \theta = \phi = 1 - y. \tag{5}$$

We perturb Eqs. (3a)–(3c) about this basic solution by setting

$$\psi = \Psi, \quad \theta = 1 - y + \Theta, \quad \phi = 1 - y + \Phi \tag{6}$$

and linearising. Hence we obtain

$$\Psi_{xx} + \Psi_{yy} = R\Theta_x, \tag{7a}$$

$$\Theta_t = \Theta_{xx} + \Theta_{yy} + \Psi_x + H(\Phi - \Theta), \tag{7b}$$

$$\alpha\Phi_t = \Phi_{xx} + \Phi_{yy} + \gamma H(\Theta - \Phi). \tag{7c}$$

The principle of exchange of stabilities (see [15]) may be shown easily, indicating that the onset of convection is stationary, or, in other words, that no travelling waves appear. Eqs. (7a)–(7c) admit solutions in the form

$$\Psi = A_1 \sin\pi y \cos kx, \quad \Theta = A_2 \sin\pi y \sin kx,$$
$$\Phi = A_3 \sin\pi y \sin kx, \tag{8}$$

where k is the horizontal wavenumber and the A-coefficients are constants. Substitution of (8) into (7a)–(7c) yields the following equation:

$$\begin{pmatrix} \pi^2 + k^2 & Rk & 0 \\ k & \pi^2 + k^2 + H & -H \\ 0 & -\gamma H & \pi^2 + k^2 + \gamma H \end{pmatrix} \begin{pmatrix} A_1 \\ A_2 \\ A_3 \end{pmatrix} = \begin{pmatrix} 0 \\ 0 \\ 0 \end{pmatrix}. \tag{9}$$

Setting the determinant of the matrix to zero yields the following expression for the value of R:

$$R = \frac{(\pi^2 + k^2)^2}{k^2}\left[\frac{(\pi^2 + k^2) + H(1+\gamma)}{(\pi^2 + k^2 + \gamma H)}\right]. \tag{10}$$

Given chosen values of H and γ, (10) describes the neutral curve for the onset of convection, the shape of which is identical *in form* to that of the Darcy–Bénard problem with LTE. By this is meant that the curve possesses one minimum, while $R = O(k^{-2})$ as $k \to 0$ and $R = O(k^2)$ as $k \to \infty$. In Fig. 1 we display neutral curves for $H = 100$ for a range of values of γ. In general R increases as γ decreases and we also see that the minimising wavenumber also increases as γ decreases. When the layer is infinite in extent the minimum value of R, denoted by R_c, is the most important value and we now concentrate on this value as a function of both H and γ. We denote by k_c that value of k which corresponds to R_c.

The value of R given in (10) may be minimised with respect to k, and, although the condition $\partial R/\partial k = 0$ may be written down, it appears to be impossible to obtain a straightforward closed-form explicit expression for the minimising value of k. Threfore we used a multidimensional Newton–Raphson iteration scheme to obtain the values of R and k as functions of H and γ. This scheme used a numerical differentiation procedure to compute

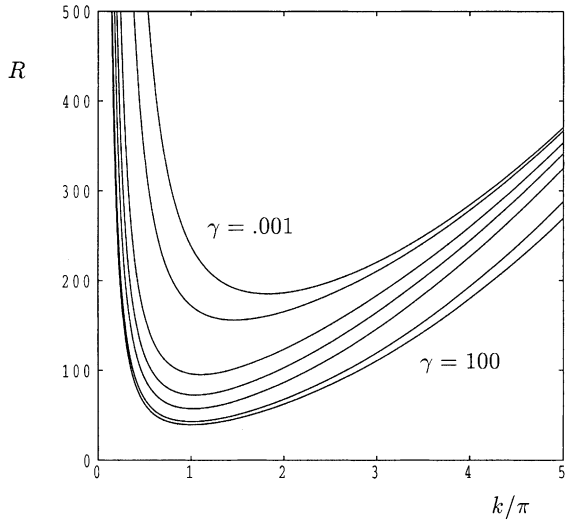

Fig. 1. Neutral curves for the onset of convection for $\gamma = 0.001$, 0.1, 0.5, 1, 2, 10 and 100 when $H = 100$.

approximate values of the iteration matrix. To illustrate the method suppose we wish to solve the system $F(\alpha,\beta)=0$, $G(\alpha,\beta)=0$ then the iteration scheme is

$$\begin{pmatrix}\alpha_{n+1}\\ \beta_{n+1}\end{pmatrix}=\begin{pmatrix}\alpha_n\\ \beta_n\end{pmatrix}-\begin{pmatrix}\partial F/\partial\alpha & \partial F/\partial\beta\\ \partial G/\partial\alpha & \partial G/\partial\beta\end{pmatrix}_n^{-1}\begin{pmatrix}F\\ G\end{pmatrix}_n,$$

where $\frac{\partial F}{\partial\alpha}|_n$ is approximated by the expression

$$\frac{F(\alpha_n+\delta,\beta_n)-F(\alpha_n,\beta_n)}{\delta}$$

and $\frac{\partial F}{\partial\beta}|_n$ by

$$\frac{F(\alpha_n,\beta_n+\delta)-F(\alpha_n,\beta_n)}{\delta},$$

where the subscript denotes iteration number, and δ takes sufficiently small values.

In Figs. 2 and 3, respectively, we show the values of R_c and $R_c\gamma/(1+\gamma)$ at the minimising wavenumber, k_c, which is depicted in Fig. 4. Note that R is the Rayleigh number which is based upon the properties of the fluid (see Eq. (4)) while

$$\left(\frac{\gamma}{1+\gamma}\right)R=\frac{\rho_f g\beta(T_l-T_u)Kd}{[\epsilon\kappa_f+(1-\epsilon)\kappa_s]\mu} \tag{11}$$

is the Rayleigh number based on the mean properties of the porous medium, and it is this latter value which is used when assuming LTE.

At small values of H we see from Fig. 2 that R_c is close to $4\pi^2$ and is independent of γ to leading order. The physical reason for this is that there is almost no transfer of heat between the phases and therefore the onset criterion is not affected by the properties of the solid phase. But at large values of H, the LTE limit, the onset criterion is based on the mean properties of the medium

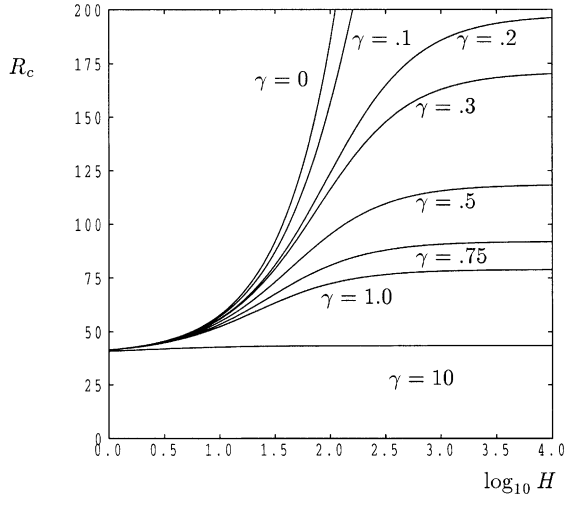

Fig. 2. Variation of R_c with $\log_{10} H$ for specific values of the parameter γ.

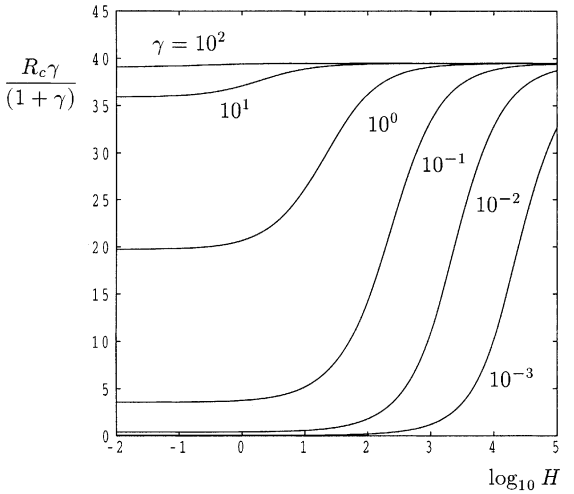

Fig. 3. Variation of $R_c\gamma/(1+\gamma)$ with $\log_{10} H$ for specific values of γ.

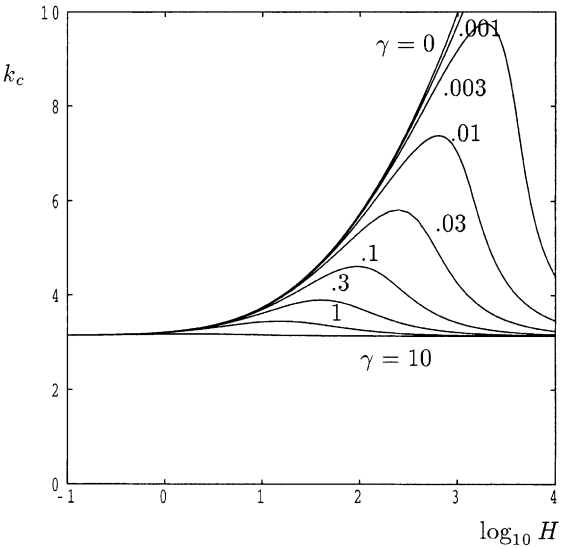

Fig. 4. Variation of the critical wavenumber with $\log_{10} H$ for specific vaules of γ.

and therefore the onset criterion in terms of R_c is dependent on γ. Fig. 3 shows that $R_c\gamma/(1+\gamma)$ has the common limit of $4\pi^2$ as $H\to\infty$, although the approach to that limit depends quite strongly on the value of γ. In all cases both R_c and $R_c\gamma/(1+\gamma)$ vary monotonically as H increases with γ fixed.

In Fig. 4 we display k_c, the minimising values of k. We see that $k_c\to\pi$ as $H\to 0$ and as $H\to\infty$; this is not surprising as the corresponding physical problems display considerable similarity. As $H\to 0$ the solid phase ceases to affect the thermal field of the fluid which is free

Table 1
Comparison of the exact and asymptotic values of H, the wavenumber, k_c, and the critical Rayleigh number, R_c, which maximise the critical wavenumber for various values of γ

γ	H (E)	H (A)	k_c (E)	k_c (A)	R_c (E)	R_c (A)
10^2	0.196657	0.196652	3.145507	3.145507	39.67538	39.67538
10^1	1.905025	1.899899	3.179696	3.179635	41.41133	41.40916
10^0	15.40310	12.33701	3.451618	3.411573	56.32689	56.89967
10^{-1}	93.98499		4.615375		151.28364	
10^{-2}	640.7896		7.384372		764.3386	
10^{-3}	5402.725	5402.959	12.69114	12.88712	5739.522	5715.063
10^{-4}	50828.39	50828.46	22.32576	22.32549	51840.03	51815.42
10^{-5}	498161.8	498161.8	39.56595	39.56590	501307.5	501282.8

'E' denotes the exact solution while 'A' denotes the asymptotic solution given by (28) and (29).

to act independently, whereas as $H \to \infty$ the solid and fluid phases may be treated as a single phase as they have nearly identical temperatures. The respective mathematical problems are identical except for a re-scaling of R.

At intermediate values of H we see that $k_c > \pi$ in all cases and that $k_c(\gamma, H)$ attains a maximum value at all non-zero values of γ. This maximum occurs at increasing values of H and k_c as $\gamma \to 0$ – this limit is considered in detail below, but values of k_c, H and R_c corresponding to such maxima are given in Table 1. When $\gamma = 0.001$, for example, $k_c \simeq 12.7$ which corresponds to tall thin cells of aspect ratio close to 4; these should be observed readily in suitable experiments.

3. Asymptotic analysis for both small and large values of H

When H is small the critical value of R_c is slightly above $4\pi^2$ which may be confirmed by minimising the small-H series expansion of (10),

$$R_c = \frac{(\pi^2 + k^2)^2}{k^2} + H\frac{(\pi^2 + k^2)}{k^2} - H^2\gamma/k^2 + \cdots, \tag{12}$$

with respect to k and by setting $\partial R_c/\partial k = 0$. Therefore we have the following expression:

$$(k^4 - \pi^4) - \pi^2 H + \gamma H^2 + \cdots = 0. \tag{13}$$

If we now substitute

$$k = \pi + Hk_1 + H^2 k_2 + \cdots \tag{14}$$

into Eq. (13), then the equating of coefficients of the same powers of H will allow us to find k_1 and k_2. Therefore we obtain

$$k_c = \pi + H/4\pi - \left(\frac{8\gamma + 3}{32\pi^3}\right)H^2 + \cdots \tag{15}$$

and hence

$$R_c = 4\pi^2 + 2H - (1 + 4\gamma)\frac{H^2}{4\pi^2} + \cdots \tag{16}$$

on using (12). Detailed quantitative comparisons between (15) and (16) and their numerical counterparts are displayed in Table 2(a) and (b) where the asymptotic solutions display six-figure accuracy when $H \leqslant 10^{-1}$.

For large values of H, R_c takes the form

$$R_c = \frac{(\pi^2 + k^2)^2}{k^2}\frac{(1 + \gamma)}{\gamma} \times \left[1 - \frac{(\pi^2 + k^2)}{H\gamma(1 + \gamma)} + \frac{(\pi^2 + k^2)^2}{H^2\gamma^2(1 + \gamma)} + \cdots\right], \tag{17}$$

which we minimise with respect to k in the same way as above. We obtain the following expression which ensures that $\partial R/\partial k = 0$,

$$\frac{(1 + \gamma)}{\gamma}(k^2 - \pi^2) - \frac{(k^2 + \pi^2)(2k^2 - \pi^2)}{\gamma^2 H} + \frac{(k^2 + \pi^2)^2(3k^2 - \pi^2)}{\gamma^3 H^2} + \cdots = 0. \tag{18}$$

If we let

$$k = \pi + \frac{k_1}{H} + \frac{k_2}{H^2} + \cdots, \tag{19}$$

then equating the coefficients of equal powers of H^{-1} allows us to find k_1 and k_2. Substitution of these values into (18) gives the following expression for critical wavenumber:

$$k_c = \pi + \frac{\pi^3}{\gamma(1 + \gamma)}H^{-1} + \frac{\pi^5}{\gamma^2(1 + \gamma)^2}\left(\frac{1 - 8\gamma}{2}\right)H^{-2} + \cdots \tag{20}$$

and hence the critical Rayleigh number is

$$R_c = \left(\frac{1 + \gamma}{\gamma}\right)4\pi^2\left[1 - \frac{2\pi^2}{\gamma(1 + \gamma)}H^{-1} + \frac{\pi^4(3 + 4\gamma)}{\gamma^2(1 + \gamma)^2}H^{-2} + \cdots\right]. \tag{21}$$

Table 2
Comparison of exact and asymptotic values of the wave number and the critical Rayleigh number for small H for $\gamma = 1.0$ and $\gamma = 0.01$

$\log_{10} H$	k_c (E)	k_c (A)	R_c (E)	R_c (A)
(a) $\gamma = 1.0$				
−2.0	3.142388	3.142387	39.498405	39.498405
−1.5	3.144098	3.144098	39.541537	39.541537
−1.0	3.149441	3.149440	39.677163	39.677151
−0.5	3.165691	3.165649	40.098560	40.098208
0.0	3.211317	3.210084	41.362100	41.351766
0.5	3.313460		44.804663	
1.0	3.436346		52.359639	
(b) $\gamma = 0.01$				
−2.0	3.142388	3.142388	39.498415	39.498415
−1.5	3.144106	3.144106	39.541637	39.541637
−1.0	3.149520	3.149519	39.678155	39.678154
−0.5	3.166453	3.166447	40.108280	40.108239
0.0	3.218239	3.218066	41.453330	41.452074
0.5	3.366995		45.574790	
1.0	3.737411		57.675516	

'E' denotes the exact solution while 'A' denotes the asymptotic solution given by (15) and (16).

Table 3
Comparison of exact and asymptotic values for wave numbers and the critical Rayleigh numbers for large H for $\gamma = 1.0$ and $\gamma = 0.01$

$\log_{10} H$	k_c (E)	k_c (A)	R_c (E)	R_c (A)
(a) $\gamma = 1.0$				
1.5	3.409561	3.364078	63.404279	69.733517
2.0	3.270609	3.269847	72.339570	72.510053
2.5	3.187952	3.187940	76.621357	76.627153
3.0	3.156828	3.156828	78.190834	78.191022
3.5	3.146468	3.146468	78.711747	78.711753
4.0	3.143140	3.143140	78.879042	78.879043
4.5	3.142083	3.142083	78.932206	78.932206
5.0	3.141748	3.141748	78.949044	78.949044
(b) $\gamma = 0.01$				
3.5	4.287406	4.250385	2336.676	2680.518
4.0	3.463536	3.462385	3310.289	3323.795
4.5	3.240088	3.240052	3752.005	3752.467
5.0	3.172431	3.172430	3910.535	3910.550
5.5	3.151314	3.151314	3962.793	3962.793
6.0	3.144664	3.144664	3979.539	3979.539

'E' denotes the exact solution while 'A' denotes the asymptotic solution given by (20) and (21).

Comparisons of k_c and R_c as given by (20) and (21) with the exact values are displayed in Table 3(a) and (b) for $\gamma = 1$ and $\gamma = 0.01$; agreement is again found to be excellent.

4. Asymptotic analysis for the maximum critical wavenumber for both $\gamma \gg 1$ and $\gamma \ll 1$

In Fig. 4 we see that there exists a maximum wavenumber for the onset of convection for each value of γ. These values have already been presented in Table 1 and were obtained by solving Eq. (10), the equation

$$(k^2 - \pi^2)\left[1 + \frac{H}{\pi^2 + k^2 + \gamma H}\right] = \frac{k^2(\pi^2 + k^2)H}{(\pi^2 + k^2 + \gamma H)^2}, \qquad (22)$$

which was obtained by taking $\partial/\partial k$ of Eq. (10) and setting $\partial R/\partial k = 0$, and the equation

$$2\gamma(\gamma + 1)H = (\pi^2 + k^2)\left[\frac{k^2}{k^2 - \pi^2} - (1 + 2\gamma)\right] \qquad (23)$$

which was obtained by taking $\partial/\partial H$ of Eq. (22) and setting $\partial k/\partial H = 0$ – this final condition is the one which corresponds to the maximum value of k shown in Fig. 4. Guided by the behaviour of the entries in Table 1 for large values of γ, we set

$$k_c \sim \pi + \frac{k_1}{\gamma} + \frac{k_2}{\gamma^2}, \quad H \sim \frac{H_1}{\gamma} + \frac{H_2}{\gamma^2},$$
$$R_c \sim 4\pi^2 + \frac{R_1}{\gamma} + \frac{R_2}{\gamma^2} \tag{24}$$

into Eqs. (10), (22) and (23). At leading order, (22) and (23) yield the equations

$$k_1 = \frac{\pi^3 H_1}{(2\pi^2 + H_1)^2} \quad \text{and} \quad k_1 = \frac{\pi^3}{2(2\pi^2 + H_1)}, \tag{25}$$

from which we deduce that

$$k_1 = \frac{1}{8}\pi \quad \text{and } H_1 = 2\pi^2. \tag{26}$$

At the next order quite lengthy expressions are obtained, but these yield the values

$$k_2 = -\frac{5}{128}\pi \quad \text{and} \quad H_2 = -\frac{3}{4}\pi^2. \tag{27}$$

On using these expressions in (24) and evaluating R_c from (10), we obtain

$$k_c \sim \pi\left[1 + \frac{1}{8}\gamma^{-1} - \frac{5}{128}\gamma^{-2}\right],$$
$$H \sim \pi^2\left[2\gamma^{-1} - \frac{3}{4}\gamma^{-2}\right], \tag{28}$$
$$R_c \sim \pi^2\left[4 + 2\gamma^{-1} - \frac{7}{16}\gamma^{-2}\right].$$

These values are displayed in Table 1 and we find agreement to at least five figures for $\gamma \geqslant 100$.

Turning to small values of γ, it is clear from the numerical data listed in Table 1 that $H = O(\gamma^{-1})$, $R_c = O(\gamma^{-1})$ and $k_c = O(\gamma^{-1/4})$ as $\gamma \to 0$. We examine this asymptotic limit using these scalings at leading order and allow the second term in the expansions for H, R_c and k_c to be of $O(\gamma^{1/2})$ magnitude relative to the leading terms. We omit the detailed analysis, but it is possible to show that

$$k_c \sim \left[\gamma^{-1/4} + \frac{1}{2}\gamma^{1/4}\right]\pi/\sqrt{2},$$
$$H \sim \left[\gamma^{-1} + 3\gamma^{-1/2}\right]\pi^2/2, \tag{29}$$
$$R_c \sim \left[\gamma^{-1} + 5\gamma^{-1/2}\right]\pi^2/2.$$

These values are also presented in Table 1; yet again comparisons are excellent and especially so for $\gamma \leqslant 10^{-4}$.

5. Conclusion

A study has been undertaken of the effects of relaxing the assumption of LTE on the onset of Darcy–Bénard convection. The neutral curve for the onset of convection retains its unimodal shape with one distinct minimum which defines the critical Rayleigh number and wavenumber. We have seen that changing the values of H and γ has a significant effect on modifying the conditions under which convection will take place. Detailed and comprehensive numerical solutions have been presented for R_c and k_c as functions of both H and γ, and these have been supplemented by asymptotic analyses in the large-H and small-H limits. We find that LTE is recovered in the large-H limit. Of particular interest is the fact that under some circumstances the critical wavenumber attains large values which corresponds to tall thin convection cells. Numerical and asymptotic analyses of this situation reveals the fact that this phenomenon occurs when H is large, γ is small, but with $H\gamma = O(1)$; it would be of very considerable interest for this unusual result to be confirmed by direct experiment.

Acknowledgements

The first-named author would like to thank the University of Bath for a Research Studentship to enable this research to be undertaken. The authors would like to thank the referees for their comments which served to improve the paper.

References

[1] E.R. Lapwood, Convection of a fluid in a porous medium, Proc. Cambridge Philos. Soc. 44 (1948) 508–521.
[2] D.A.S. Rees, I. Pop, Free convective stagnation-point flow in a porous medium using a thermal nonequilibrium model, Int. Commun. Heat Mass Transfer 26 (1999) 945–954.
[3] D.A.S. Rees, I. Pop, Vertical free convective boundary-layer flow in a porous medium using a thermal nonequilibrium model, J. Porous Media 3 (2000) 31–44.
[4] D.A.S. Rees, Vertical free convective boundary-layer flow in a porous medium using a thermal nonequilibrium model elliptic effects, J. Appl. Math. Phys. (ZAMP) (2002), to appear.
[5] D.A. Nield, A. Bejan, Convection in Porous Media, second ed., Springer, Berlin, 1998.
[6] M. Quintard, M. Kaviany, S. Whitaker, Two-medium treatment of heat transfer in porous media: numerical results for effective properties, Adv. Water Resour. 20 (1997) 77–94.
[7] K. Vafai, A. Amiri, Non-Darcian effects in confined forced convective flows, in: D.B. Ingham, I. Pop (Eds.), Transport Phenomena in Porous Media, Pergamon Press, Oxford, 1998, pp. 313–329.
[8] D. Nield, A.V. Kuznetsov, The interaction of thermal nonequilibrium and heterogeneous conductivity effects in forced convection in layered porous channels, Int. J. Heat Mass Transfer 44 (2001) 4369–4373.
[9] V.V. Calmidi, R.L. Mahajan, Forced convection in high porosity foams, Trans. ASME J. Heat Transfer 122 (2000) 557–565.

[10] Carbonell, S. Whitaker, Heat and mass transfer in porous media, in: J. Bear, M.Y. Corapcioglu (Eds.), Fundamentals of Transport Phenomena in Porous Media, NATO ASI Series E: Applied Sciences, Barking,, vol. 82, 1982, pp. 123–198.
[11] C.W. Horton, R.T. Rogers, Convection currents in a porous medium, J. Appl. Phys. 16 (1945) 367–370.
[12] M. Combarnous, Description du transfert de chaleur par convection naturelle dans une couche poreuse horizontale á l'aide d'un coefficient de transfert solide–fluide, C. R. Acad. Sci. Paris II, Ser. A 275 (1972) 1375–1378.
[13] M. Quintard, Modelling local non-equilibrium heat transfer in porous media, in: Proc. 11th Int. Heat Transfer Conf., Kyong-ju, Korea, August 1998, vol. 1, 1998, pp. 279–285.
[14] S.J. Kim, D. Kim, Thermal interaction at the interface between a porous medium and an impermeable wall, Trans. ASME J. Heat Transfer 123 (2001) 527–533.
[15] P.G. Drazin, W.H. Reid, Hydrodynamic Stability, Cambridge University Press, Cambridge, MA, 1981.